Journal of Materials Science: Materials in Medicine (2025)36:29
https://doi.org/10.1007/s10856-025-06875-6

BIOMATERIALS SYNTHESIS AND CHARACTERIZATION

Original Research

Hybrid fibres: a new path in tissue regeneration

Johana Kulhánková[1] · Christopher J. Hobbs[2] · Barbora Nikendey Holubová[2] · Jakub Erben[3] · Miroslava Rysová[4] · Jana Musílková[5] · Lucie Svobodová[5] · Nataliya Romanyuk[6] · Veronika Máková[2]

Received: 22 September 2024 / Accepted: 3 March 2025

Abstract

Nowadays, various forms of organosilane materials are well established in the field of regenerative medicine, but interestingly, fibrous organosilanes have yet to be described. So far, technological obstacles prevent the preparation of such fibrous materials without any presence of spinnability-supporting organic polymers, various types of surfactants, or non-polar organic solvents, which are in many cases highly toxic and economically inconvenient. Recently, these obstacles were overcome by a complex, yet simple, technology combining different science perspectives from supramolecular chemistry through material science to tissue engineering. This paper suggests a synthesis of two biomedically promising monomeric organosilane precursors, *N*,*N*´-**b**is(3-(**t**riethoxysilyl)propyl)**t**erephthalamide (**BTT**) and *N*,*N*´-**b**is(3-(**t**riethoxysilyl)propyl) **p**yridine-2,6-dicarboxamide (**BTP**), which are submitted to a sol-gel process combined with subsequent electrospinning technology. Such a unique procedure not only allows the preparation of toxic-free organosilane fibrous mats by suitable adjustment of sol-gel and electrospinning parameters but also simplifies material production via a one-pot synthesis approach further tuneable with appropriate organosilane precursors. The BTT and BTP fibrous materials prepared displayed not only a promising interface among the materials and 3T3 fibroblast cell lines but moreover, the interaction of nanofibrous materials with stem cells has yielded encouraging outcomes. Stem cell adhesion, proliferation, and differentiation were notably enhanced in the presence of these materials, suggesting a supportive microenvironment conducive to regenerative responses. The ability of the material to modulate the cellular behaviour of stem cells holds promising implications for the development of targeted and effective regenerative therapies.

✉ Veronika Máková
veronika.makova@tul.cz

[1] Faculty of Science, Humanities and Education, Technical University of Liberec, Studentská 1402/2, 461 17 Liberec, Czech Republic

[2] Department of Nanochemistry, Institute for Nanomaterials, Advanced Technologies and Innovation, Technical University of Liberec, Studentská 1402/2, 461 17 Liberec, Czech Republic

[3] Department of Nonwovens and Nanofibrous Materials, Faculty of Textile Engineering, Technical University of Liberec, Studentská 2, 461 17 Liberec, Czech Republic

[4] Department of Applied Biology, Institute for Nanomaterials, Advanced Technologies and Innovation, Technical University of Liberec, Studentská 1402/2, 461 17 Liberec, Czech Republic

[5] Institute of Physiology, Czech Academy of Science, Vídeňská 1083, 142 20 Prague, Czech Republic

[6] Department of Neuroregeneration, Institute of Experimental Medicine, Czech Academy of Science, 142 20 Prague, Czech Republic

Published online: 26 March 2025

Graphical Abstract

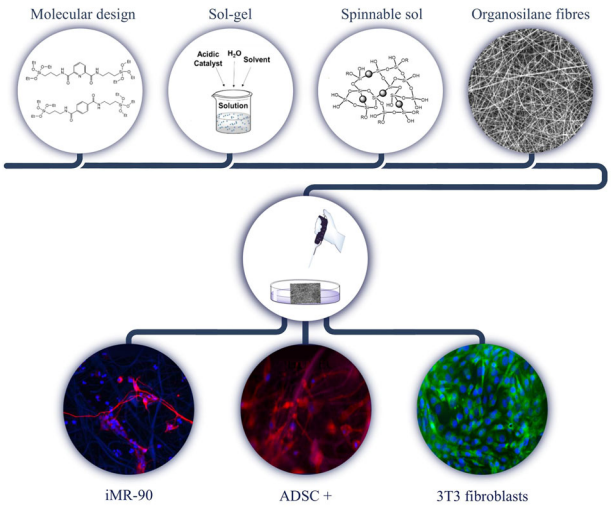

1 Introduction

The development of the human cortical system is characterised by a series of highly regulated, dynamic processes beginning with the generation of neuroepithelial stem cells and resulting in formation of neural circuits [1]. The process of any therapy, treatment or regeneration is then very complicated. Thus, as the neurodegenerative diseases became a burning issue in society, the need of designing eligible therapeutic solutions employed many scientists and doctors worldwide [2]. Revolutionary changes in comprehension of human neurogenesis were made with the discovery of multipotent stem cells in the adult's brain. The discovery changed the long accepted theory about regeneration and/or growth of the neural system throughout adult life and started a whole new discipline of therapeutic possibilities [3–5].

Neuroregenerative medicine stands at the forefront of scientific exploration, seeking to address the intricate challenges associated with the repair and regeneration of the central nervous system [6]. Materials for these purposes have to be carefully selected and engineered to navigate the complex landscape of the nervous system. Synthetic polymers, biocompatible scaffolds, and nanomaterials take centre stage, each designed with precision to mimic the intricate architecture of neural tissues. These materials should not only provide physical support but also create an environment that encourages axonal growth, neuronal migration, and the establishment of functional neural connections [7–9].

Nowadays, conductive polymers are used as biomaterials for electrically stimulating neural cells. They are given significant interest because of their versatility [10] and ability to interface with neural tissue [11]. However, commonly used conductive polymers such as polypyrrole (PPy) and poly(3,4-ethylenedioxythiophene (PEDOT) often display poor mechanical properties or processability [12]. Nevertheless, many researchers around the world are interested in PPy, becoming one of the most widely investigated conductive polymers [13, 14].

Significant discoveries have been made in the development of graphene-based materials [15]. The main advantages of these materials lie in the enhancing of mechanical properties compared to the already studied materials [16]. Together with high electric conductivity and flexibility in the manufacturing process appears as a suitable candidate for neural tissue [17]. Nevertheless, according to the provided cytotoxicity testing, toxicity of graphene-based materials is dependent on many factors such as shape, size, purity, post-production processing steps, oxidative state, functional groups, etc., which is highly problematic for regenerative medicine and further investigation needs to be processed [18].

In recent years, doped hydrogels with carbon-based materials have been introduced. These materials seem to offer a versatile possibility by using hydrogel´s properties with the advantages of conductive materials [19, 20]. They are promising candidates for uses in tissue regeneration thanks to their 3D porous structure with mechanical properties enhanced by carbon-based nanoparticle filling. However, the potential cytotoxicity, genotoxicity or carcinogenicity of integrated nano-sized particles and their release during the degradation of the hydrogel is a highly discussed topic and further research is necessary for this field [21].

The advent of nanotechnology has the potential to revolutionise many areas of human activities and further propel the field of neuroregenerative medicine, enabling the development of nanomaterials that can precisely manipulate

cellular behaviour and deliver therapeutic agents with unprecedented precision [22–24]. Especially nanofibres provide unique opportunities to be designed in a structural similarity to native neural tissue which is in a nanoscale range [25]. The use of nanofibres in tissue restoration is expected to result in an efficient, compact organ and rapid recovery due to their large surface area. Such structural organisation can support the cell growth together with the enabling of nutrients movement [26].

As researchers continue to push the boundaries of material science and regenerative medicine, the synergy between innovative materials and biological systems promises to unlock novel therapeutic possibilities, bringing us closer to a future where damaged tissues can be repaired and organs regenerated with unprecedented precision [27]. The formation of a suitable and functional biomaterial for neuroregenerative purposes is a vital factor that should be closely interconnected by a combination of a strong support, providing a viable environment for cell growth, possessing high surface area and structural variability of the proposed material. Only thus, this material is able to provide desirable physical conduits and support electrical signals transport together with communication between neurons [1, 26].

Herein, we introduce an entirely new class of fibrous hybrid organosilane materials having extraordinary properties that pure organic and/or inorganic materials cannot reach. In the name of the proverb that there is strength in simplicity, we suggest a one-pot preparation of purely organosilane fibrous mats based on previously designed and synthesised suitable biocompatible bridged organosilane precursors - *N,N´*-bis(3-(triethoxysilyl)propyl)terephtalamide (BTT) and *N,N´*-bis(3-(triethoxysilyl)propyl)pyridine-2,6-dicarboxamide (BTP). Such fibrous scaffolds are produced effectively and economically through the sol-gel process and suitable electrospinning techniques just on the basis of the right processing parameters. Moreover, the crucial advantage of our system lies in the ability to omit harmful and/ or toxic solvents, inorganic additives and organic polymers commonly used as spinnability facilitators to produce similar materials. All the statements mentioned above are supported by the wide range of in vitro experiments with several types of cells, including neural precursors. Thus, these experiments highlight a noteworthy success in developing distinct materials particularly appropriate for the attachment and growth of neural cells, making organosilane fibres a promising material for nervous tissue regeneration.

2 Materials and experimental methods

2.1 Materials

Following chemicals: triethylamine (TEA; Aldrich, CZ), (3-aminopropyl)triethoxysilane (APTES 99%; TCI Chemicals, CZ), terephthaloyl chloride (99% Aldrich, CZ), 2,6-pyridinedicorbonyl dichloride (99%; Aldrich, CZ), anhydrous $MgSO_4$ (Lach:Ner, CZ), toluene (99%; Lach:Ner, CZ), HCl (35%; Lach:Ner, CZ), ethanol (98%; Penta, CZ) were used as received without further processing. When dry Toluene was needed, Toluene (99%; Penta, CZ) which had been left over molecular sieves (4 Å; Acros Organics) was employed.

2.2 Synthesis

Both hybrid organosilane precursors (*N,N´*-bis(3-(triethoxysilyl)propyl)terephthalamide (BTT) and *N,N´*-bis(3-(triethoxysilyl)propyl)pyridine-2,6-dikarboxyamide (BTP) were synthesised in a 2-necked round bottom flask. Before use, the flask was dried for 3 hours at 120 °C, sealed and subjected to several vacuum/argon cycles. In the final stage, the argon was introduced into the flask and cooled to the laboratory temperature. Dry toluene (3.29 mol) was added into the flask together with terephthaloyl chloride or 2,6-pyridinedicarbonyl dichloride (0.05 mol) and stirred at 350 RPM. After dissolution, TEA (0.15 mol) was added to the mixture which was kept around 0 °C using an ice bath. Dropwise, APTES (0.10 mol) was slowly added to the mixture, turning the reaction colour to the yellow. The reaction flask was after left stirring at room temperature at 350 RPM for 3 h. The final solution was then interfused with 300 ml of Milli-Q water and separated, with the organic phase collected and the process repeated 2 times before finally obtaining the organic phase product over anhydrous $MgSO_4$. The remaining solvents were removed under reduced pressure, with 100 ml of toluene then added to the product and mixed before removal of solvent once again, with this process repeated 3 times. 50 ml of toluene was then added and filtered through a paper membrane filter followed by filtering with a 0.22 µm PVDF syringe filter. Finally, the remaining solvent was removed under reduced pressure at 80 °C for 10 h, producing a viscous yellow compound with an obtained yield of 85.9% of BTT and 91.2% of BTP. The precursors were stored in a fridge under argon atmosphere until use. The structures were confirmed using mass spectroscopy (Sciex X500R QTOF HR, USA) and NMR (400 MHz; JEOL, Japan) at 25 °C.

2.3 Sol-gel processing

The sol-gel process was carried out the same as mentioned in previous studies [28]. To form a colloidal solution (sol), one-pot synthesis was utilised. The principle of such reaction lies in mixing all chemicals (organosilane precursor, solvent, water and acid catalyst) in a round-bottom flask, heating and stirring for a certain time interval at room temperature. After homogenisation of the sol and adjusting the pH ~ 2, the flask is heated in an oil bath and refluxed

Table 1 Parameters of Nanospider™ device used in forming of organosilane fibres in 100 mol% ratio

Distance between electrode and collector [mm]	Voltage [kV]		Speed of cartridge [mm/s]	Temperature [°C]	Relative Humidity [%]
	Electrode	Collector			
160	<40	>−20	<340	<24	>30

while mixing for 350 RPM. It is important to observe the growth of the polysiloxane matrix during the whole process of heating and stirring at the appropriate time, before the structure grows too much within the 3D network or before the sol enters the gel phase. The suitable polymerisation process evolution is confirmed using FTIR spectroscopy. The final sol is then adjusted to the viscosity around 60 mPa.s and ready to be electrospun.

2.4 Electrospinning

Hybrid organosilane fibres were prepared using two different electrospinning techniques. First, in laboratory scale, the needle jet technique was used for spinability evaluation and optimization of sol properties and spinning process. The final, concentrated sol was fed into the syringe (5 ml) with a dosing needle (thickness 1.2 mm). A needle was inserted into the linear dispenser (ONE Syringe Pump; Darwin Microfluidics, FR) with feeding rate 1.5–5 ml/h. The interval distance between needle and collector moved from 15 up to 25 cm. Voltage for needle electrospinning was in the range 20–30 kV. Likewise, the Nanospider™ NS 1WS500U (Elmarco, CZ) needleless electrospinning device for industrial production of nanofibres was used to examine fabrication of such fibres in higher amounts in for of 2D homogenous fibre sheets. The climatic conditions during all experiments were regulated by a precisely controlled air conditioning system NS AC150 1000/2000 (Elmarco, CZ). Parameters for using the Nanospider™ device are listed in Table 1.

2.5 Characterization

2.5.1 Liquid-state Nuclear Magnetic Resonance (lsNMR)

Liquid NMR spectra were recorded on a JEOL spectrometer JNM-ECZ400R/M1 (400 MHz, Japan), with the chemical shifts (δ) for ^{1}H and ^{13}C spectra (recorded at 399.78 and 100.53 MHz respectively) referenced to the signals from non-deuterated residual solvent (DMSO δ_H 2.50, δ_C 39.52). Analysis of the obtained spectra was analysed using MestReNova software (V. 14.3.1 Mestrelab research).

2.5.2 FTIR spectroscopy

The sol-gel reaction was assessed periodically using FTIR Spectrometer Nicolet iZ10 (Thermo Fisher Scientific, USA) with an ATR diamond crystal angle of 45° and a spectral range of 4000–400 cm^{-1}, with 16 sample scans, 32 background scans, a resolution of 2 cm^{-1}, apodization: Happ-Genzel, atmospheric suppression correction and baseline. All liquid samples were analysed after the evaporation of ethanol.

2.5.3 Scanning electron microscopy (SEM)

Prepared fibres were studied by SEM (ZEISS, Sigma Family, DE). All of the samples were sputtered with a 2-nm platinum layer, and were subsequently viewed as secondary electron images (28 kV). The fibre diameter was characterised using NIS Elements software (LIM, CZ) and was assessed from a total of 200 measurements from 10 independent images.

2.5.4 Thermogravimetric analysis coupled with FTIR spectroscopy

Samples were analysed using a Q500 thermogravimetric analyser (TA Instruments, New Castle, USA). Samples were placed on a platinum pan and analysed in an inert atmosphere of nitrogen with a flow rate of 60 $ml.min^{-1}$. The samples were heated at 10 °C.min^{-1} from RT to 850 °C. When TGA was run in tandem with FTIR Nicolet IS10 (Thermo Fisher Scientific, USA), a transfer line heated to 220 °C from the TGA furnace connected to a 20 cm quartz cuvette heated to 240 °C was used for FTIR analysis of the TGA heat decomposition by-products.

2.5.5 Solid-state Nuclear Magnetic Resonance (ssNMR)

Solid-state (SS) NMR spectra were measured at 9.39 T using a JEOL JNM-ECZ400R/M1 NMR spectrometer (400 MHz, JEOL, Japan). Dry sample for measurement was packed into a 3.2 mm ZrO_2 sample tube rotor with spectra recorded at ambient temperature. Solid-state ^{13}C (100.53 MHz) spectra were referenced externally to γ-glycine (174.1 ppm), with spectra obtained utilising CP/MAS (with high-powered ^{1}H decoupling) at 20 kHz using optimised relaxation delays of 2 s and a contact time of 2.0 ms. Solid-state ^{29}Si (79.43 MHz) spectra were referenced externally to tetrakis(trimethylsilyl) silane (−9.8 ppm), with spectra obtained utilising CP/MAS (with high-powered ^{1}H decoupling) at 6 kHz using optimised relaxation delays of 2 s and a contact time of 5.0 ms. Spectra were subsequently analysed using MestReNova software (V. 14.3.1 Mestrelab Research).

2.5.6 Biocompatibility in vitro

Initial biocompatibility screening was performed in compliance with the standard ISO 10993-5: Biological evaluation of medical devices - Tests for in vitro cytotoxicity, using 3T3-A31 murine fibroblasts. Cell viability upon exposure in direct contact was evaluated by standard MTT test and extended to include cell membrane disruption examination through spontaneous LDH leak test. Cell morphology was monitored at all time points (24, 48 and 72 hours) by fluorescent microscopy. In general, cells were cultured under standard conditions (5% CO_2, 37 °C) in complete culture medium containing high glucose Dulbecco ′s modified Eagle′s medium (DMEM, Sigma-Aldrich, USA) supplemented with 5% fetal bovine serum (FBS, Gibco), 5% new-born calf serum (NBCS, Sigma-Aldrich, USA) and 1% penicillin-streptomycin (P/S, 10.000 U, Sigma-Aldrich, USA). Cytotoxicity study was performed in 24-well format. For the exposure, 30.000 cells were seeded per well and cultured 24 hours prior to the experiment. On the day of exposure, culture medium with unattached cells was discarded, circular sections of nanofibrous sheets (10 mm diameter) were placed directly on the bottom of each well and 1 ml of fresh complete medium was added. Each sample was tested in triplicate. Positive control (7% DMSO) and cell control were handled and tested under the same conditions. In the selected time points (24, 48 and 72 hours) culture medium was collected for the LDH leak test and cell viability of adhered cells was tested by standard mitochondrial oxidoreductases activity test using MTT assay (1 mg/ml, serum-free medium, 120 minutes). The degree of MTT reduction was determined spectrophotometrically by absorbance intensity reading at 570 nm (background subtracted at 650 nm) on SynergyHTX multi-plate reader (BioTek). The percentage of viable cells was calculated as cell control (CC, considered 100%) absorbance proportion and statistically analysed. The lactate dehydrogenase (LDH) spontaneously released to the culture medium during the exposure period was tested by CyQUANT™ LDH Cytotoxicity Assay (Invitrogen, Thermo Fisher Scientific, USA) according to manufacturer's instructions. The substrate colour reaction was measured spectrophotometrically at 490 nm (background subtracted at 680 nm) on a multi-plate reader. The percentage of LDH in culture media as a sign of cellular membrane disruption was calculated as the absorbance proportion of completely lysed population (at corresponding time point) after subtracting culture medium control values. Results were statistically analysed.

For the cell morphology evaluation, cells were seeded on round coverslips (12 mm) and treated under the same conditions. After the exposure period, cells were washed with Dulbecco′s PBS solution (DPBS, pH 7.4), fixed with ice-cold methanol and stained with DiOC6(3) (0.1 µg/ml) for 45 minutes in the dark. Cell nuclei were counterstained with DAPI using Fluoroshield™ mounting medium (Sigma-Aldrich, USA). The imaging was carried out on MDi8 inverted microscope (Leica) using HC FL PLAN objective and integrated LAS X system.

Quantitative data obtained by biocompatibility testing were statistically analysed and presented as mean values ± standard deviation (SD). Results were evaluated statistically using GraphPad Prism 8.4.2. The normality of the data was tested by the D'Agostino-Pearson test or the Shapiro-Wilk test. If the data passed the normality test, statistical significance between control and groups was determined by ANOVA with Dunnett´s comparative test (p set to 0.05) or by Brown-Forsyth and Welch ANOVA with Dunnetts T3 multiple comparison test (p set to 0.01) for pairs of groups.

2.5.7 Cell cultivation on tested samples

The sample's biocompatibility and surface cell adhesion were further tested by three types of human stem cells: Adipose-derived Stem Cells (ADSC) for basic estimations, Human Umbilical Vein Endothelial Cells (HUVEC) alone or co-cultivated with ADSC for possible utilisation for soft tissue reconstruction, and after all human neural stem cells, induced pluripotent stem cell derived neural precursors (iPSC-NPs) IMR-90 cell line for possible utilisation for neural tissue reconstruction. All cells were cultivated under static conditions in 24-well polystyrene plates (Techno Plastic Products, Switzerland). The cells were seeded in a density of 25 000 cells/cm^2 and cultivated in a humidified air atmosphere with 5% CO_2, and at 37 °C in a cell incubator (Thermo Fisher Scientific, USA). The cultivation medium depended on the cell type.

The human Adipose-derived Stem Cells (ADSC) were isolated from lipoaspirate according to our earlier study [29]. In passage 2, the cells were characterised by flow cytometry (Accuri C6 Flow Cytometer) for the presence of markers typical for mesenchymal stem cells (CD105, CD90, CD73, CD29) and absence of markers of other cell types, such as hematopoietic cells and endothelial cells (CD45, CD34, CD31). The ADSC were grown in Dulbecco's Modified Eagle Medium (DMEM), supplemented with 10% of fetal bovine serum (FBS; both by Gibco, Thermo Fisher Scientific), 1% of ABAM antibiotics (100 IU/mL of penicillin, 100 µg/mL of streptomycin, and 0.25 µg/mL of Amphotericin B; Sigma-Aldrich, USA) and basic fibroblast growth factor (FGF2; 10 ng/mL, GenScript).

Primary Human Umbilical Vein Endothelial Cells (HUVEC) (PromoCell, Germany) were isolated from the vein of the umbilical cord which are commonly used for physiological and pharmacological investigations. They express endothelial markers CD31/105. Cells were cultivated in Endothelial Growth Medium 2 (EGM-2)

(PromoCell, Germany), a low serum cell culture medium containing 2% of FS. Also, in case of co-cultivation with ADSC the cell type mix was cultivated in EGM-2.

The human neural stem cells (NSC), iPSC line was used, derived from female foetal lung fibroblasts (IMR-90 line, ATCC, USA) transduced with a lentivirus-mediated combination of OCT4, SOX2, NANOG and LIN28 human cDNA [30]. Clone selection, validation of the iPSC line and derivation of neuronal precursors are described in detail in [31]. Human induced pluripotent stem cell-derived neural precursors (iPSC-NPs) were routinely cultured in tissue culture flasks coated with poly-L-ornithine (0.002% in distilled water) and laminin (10 µg/ml in DMEM:F12), both obtained from Sigma (St. Louis, MO). NSC culture medium comprised of DMEM/F12 and Neurobasal media mixture (1:1) supplemented by B27 and N2 supplements (GIBCO, Life Technologies, Grand Island, NY), penicillin and streptomycin (50 U/ml, GIBCO), FGF (10 ng/ml), EGF (10 ng/ml) and BDNF (20 ng/ml) (PeproTech, London, UK) was replaced every second day.

Prior to the cell seeding, the tested materials were sterilised by UV and inserted into wells of 24-well polystyrene plates (TPP, Trasadingen, Switzerland, inner well diameter 1.5 cm). ADSC were seeded on the materials in a seeding density of 25 000 cells/cm^2 (50 000 cells/sample) and cultured for 3 days in DMEM cultivation medium (Sigma-Aldrich, MO, U.S.A), supplemented with 10% fetal bovine serum (FBS; Sebak GmbH, Aidenbach, Germany) and gentamicin (40 µg/ml, LEK, Ljubljana, Slovenia) at 37 °C in an air atmosphere with 5% CO_2. iPSC-NPs were seeded on the materials in a density of 60 000 cells/cm^2 (120 000 cells/sample) and cultured for 3 days in NSC culture medium at 37 °C in an air atmosphere with 5% CO_2. Samples were tested in triplicates.

The cell number was evaluated on day 3 after cell seeding. The cells on the samples were rinsed with phosphate-buffered saline (PBS) and fixed with 4% paraformaldehyde for 15 min. The cell nuclei were visualised by a method of fluorescence DNA staining using DAPI (Sigma Aldrich) for 1 hour and photographed by an Olympus IX71 epifluorescence microscope (objective 10x), equipped with a DP 70 digital camera (both from Olympus, Japan), each sample in 10 visual fields. The cell number was counted from microphotographs automatically by the Fiji ImageJ software.

The cell morphology and spreading of ADSC were evaluated by the filamentous actin (F-actin), visualised by staining cells with phalloidin conjugated with tetramethylrhodamine (TRITC) (Sigma-Aldrich, MO, U.S.A., Cat. No. P1951), in order to evaluate the assembly of actin cytoskeleton and the shape and spreading of cells on the tested materials. The cell nuclei were counterstained by DAPI (1:200). The samples were stained for 1 hour at room temperature, rinsed with PBS. Fluorescent images were acquired by an Olympus IX71(Obj. 20x).

The growth and differentiation of NSCs were analysed using immunofluorescent labelling for βIII-tubulin, nestin and GFAP. For immunofluorescent staining, cells grown on nanofibres were fixed in 4% paraformaldehyde in PBS for 15 min, washed with 0.1 M PBS and treated with Triton X-100 (0.5%) in PBS. After blocking with normal goat serum (10% in PBS) NSCs were incubated with antibodies to βIII-tubulin (1:200), nestin (1:2000), or GFAP (1:200) diluted in PBS containing 1% BSA and Triton X-100 (0.5%). This was followed by incubation in a secondary goat anti-mouse IgG antibody conjugated with Alexa-Fluor 594 (1:400) or goat anti-rabbit IgG antibody conjugated with Alexa-Fluor 488. The nuclei were visualised using DAPI (1:200). Fluorescent images were acquired by LSM 810 DUO laser scanning confocal microscope (Zeiss).

The cell metabolic activity, which demonstrates the cell surviving on tested samples and is regarded as an indirect marker of the number and proliferation activity of cells, was estimated spectrophotometrically on day 3 after cell seeding. Conversion of resazurin (Cat. No. R7017, Sigma-Aldrich) was used to measure a metabolic activity of the cells which is considered as an indirect indicator of cell proliferation. The principle of this redox indicator assay is based on the colorimetric conversion of blue resazurin to pink resorufin which can be quantified by fluorescence or absorbance measuring. This reduction is brought about by the activity of mitochondrial enzymes of the viable cells. In brief, the stock resazurin solution (4 mM) was added to DMEM without phenol red to a final concentration of 40 µM. The cells were rinsed with PBS and the resazurin solution was added to the cells in each well and incubated with the reagent for 3 hours at 37 °C. The absorbance was measured (Ex/Em = 530/590 nm) using the VersaMax ELISA microplate reader (Molecular Devices LLC, Sunnyvale, CA, USA). A background control (resazurin solution without cells) was subtracted.

Quantitative data were analysed and presented as mean values ± standard deviation (SD). Statistical significance between groups was determined by ANOVA (Student-Newman-Keuls method) with p value set to 0.05.

3 Results

3.1 Preparation of hybrid organosilane fibres

Both precursors (BTT, BTP) were synthesised as mentioned in chapter 2.2. To observe the purity and structure of both prepared precursors, several characterisation techniques were employed. Both precursors were confirmed using mass spectroscopy and liquid-state ^{1}H-NMR (400 MHz, DMSO-d).

After the structural confirmation, an electrospinable polymeric solution (sol) was prepared by suitable adjusting of several sol-gel parameters [32]. Sol-gel process is a commonly used technique regarding the preparation of materials by mild conditions with possible control of the final product. In general, it is a process in which the transformation of monomers into the colloidal suspension (sol) occurs followed by the formation of a continuous network enclosing the liquid phase (gel) by condensation reactions [32]. According to the common theory, the sol appears to be spinnable when branching of the forming structure is relatively low and formation of long linear macromolecules is supported. Considering the reaction mechanism described in several studies [33], acid-catalysed reaction was employed (the pH was set ~ 2 using HCl). To initiate hydrolytic reactions water needs to be added to the sol, however, water and organosilane precursors are immiscible. In addition, a right type and amount of solvent to prevent steric hindrance and agglomeration together with molecular congruence of leaving group from organosilane. Hence, the proper choice of a solvent belongs to one of the crucial parameters, ethanol was chosen as a suitable solvent in large excess to the other precursors of the sol-gel reaction. Along with the choice of catalyst, type and amount of solvent, it is also important to choose a substoichiometric amount of water relative to the amount of silane precursor to control the sol-gel reaction in terms of spinnable sol formation (low branching and linearity).

Reaction time of sol-gel electrospinnable systems was not thoroughly studied yet therefore it was set experimentally while observing using FTIR spectra. Using infrared spectroscopy, changes in the structure of a sol can be detected while observing fingerprint regions of characteristic areas for the following functional groups (Si-OH/H_2O, Si-OR, -Si-O-Si-). As evident from Fig. 1, the polycondensation reaction is marked by an increase in intensity and broadening of the peaks at approximately 1150 cm^{-1}, indicating the formation of -Si-O-Si- bonds. Additionally, there is a decrease in -Si-OH signals at around 950–900 cm^{-1}, indicating the development of the polysiloxane network and further indicating the subsiding hydrolysis due to the occurring polycondensation process [34, 35]. This is also accompanied by a significant decrease in the intensities of the bands at around 3700–2800 cm^{-1} attributed to the H_2O/Si-OH and aliphatic groups (water and ethanol are products of the polycondensation reactions). When the sol-gel reaction is stopped, the ratio between Si-OH and formed polysiloxane unit no longer changes and the band of Si-OH units at around 950 cm^{-1} is still very distinctive with a blue shift to higher wavenumbers marking the higher network organisation, but with lower 3D branching [34, 35]. Subsequently, the excess solvent needs to be distilled, and the sol has to be adjusted to the suitable viscosity of 40–60 mPa.s. Prepared sol was then electrospun using techniques described in chapter 2.4.

3.2 Characterisation techniques

All electrospun fibres prepared according to the above-mentioned sol-gel process and subsequent electrospinning were analysed using various characterisation techniques with the aim of confirming the successful preparation of smooth homogenous fibres without any inhomogeneities (SEM) as well as their linear, low branched structure (ssNMR, Raman, FTIR). There were also several characterisation experiments determining their closer specification (TGA, contact angle, conductivity measurement etc.).

According to the obtained SEM images (Fig. 2), the reported pathway was set to result in smooth, homogenous, morphologically compact fibres. The size of fibrous diameters ranged from hundreds to thousands of nanometres with an average size 1117.6 nm for BTT fibres and 967.3 nm for BTP fibres.

When proof of smooth, long and continuously deposited fibres was obtained, several structural characterisation techniques were utilised. First, the ssNMR spectra were assessed. In regard to observing possible changes in the organic part of the molecule, the ^{13}C ssNMR (Fig. 3) was embraced. The spectra align well with the expected polymer structure from the precursor material, with only significate decrease in peak intensities corresponding the -O-CH_2-CH_3 and -CH_2-CH_3 signals in the structure. This is expected due to the polycondensation process employed removing ethyl groups from the material. Well-preserved aromatic spacer containing diverse heteroatoms may act in a favour to resulting conductive properties as well as a formation of various non-covalent interactions during the fibre-making process (the π-π stacking, etc.).

^{29}Si ssNMR measurements were also used to further observed the polycondensation of polysiloxane network units (Fig. 4), with three signals T^1 (−55 ppm), T^2 (−65 ppm) and T^3 (−74 ppm) identified. The degree of polycondensation of BTT fibres was determined to be 0.69 and for BTP fibres 0.63. The relative amount of unreacted ethoxy groups is lower within BTP fibres. From this point of view, both structures are rather linear and low branched (T^3 units = 14.8 resp. 9.9) confirming the suitable adjustments in sol-gel process of spinnable sols.

Thermal stability of prepared fibres corresponds to the thermal stability of synthesised organosilane precursors (decomposition of the main part of the precursor 60 wt.% and 94 wt.% occurs around 240 °C). Formed fibres show slightly higher thermal stability likely due to the induced cross-linking via the polycondensation reactions.

3.3 Biological assessment

3.3.1 In vitro biocompatibility evaluation on 3T3 fibroblasts

The initial biocompatibility screening on 3T3 murine fibroblasts comprised of cell viability evaluation after 24, 48 and

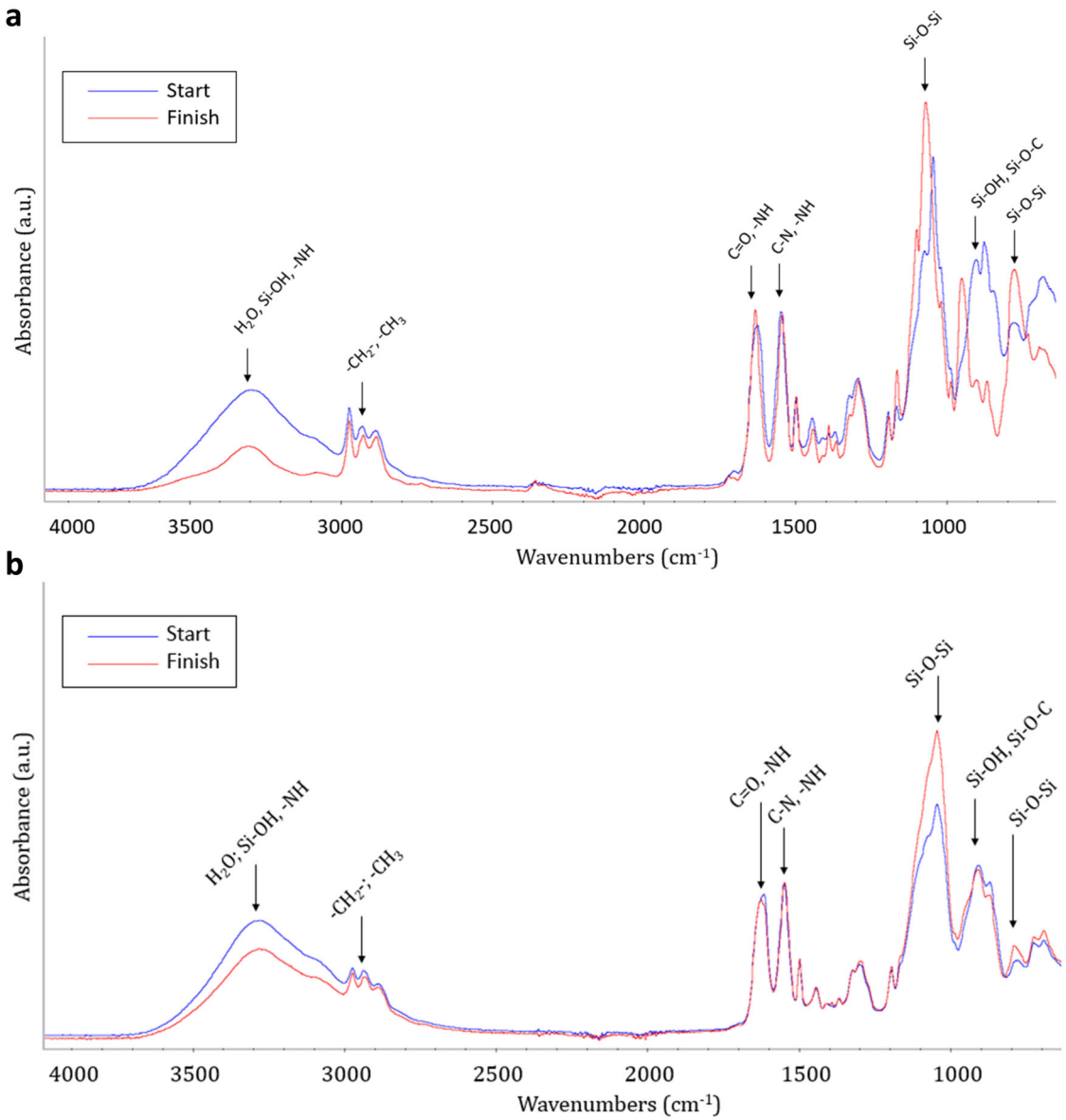

Fig. 1 FT-IR spectra of BTT (**a**) and BTP (**b**) before (blue line) and after 1 hour (red line) of the running sol-gel process focusing on the fingerprint regions characteristic for the structural changes in the system

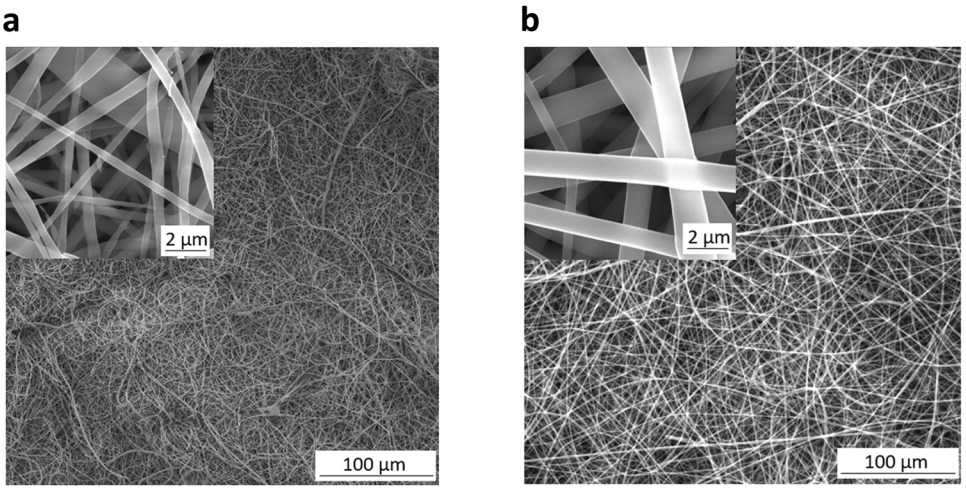

Fig. 2 SEM images BTT (**a**) and BTP (**b**) fibres from Nanospider™

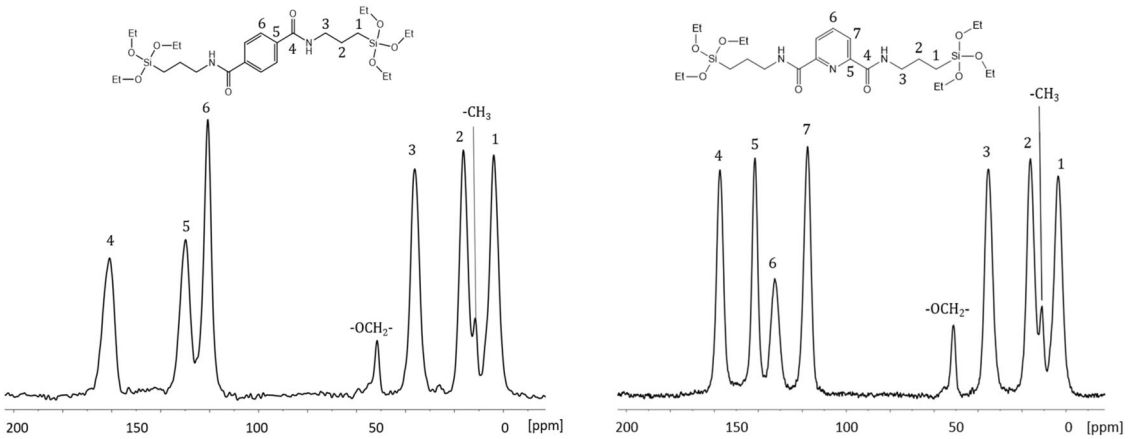

Fig. 3 ^{13}C CP/MAS NMR spectra of fibrous materials created from BTT and BTP organosilane precursor

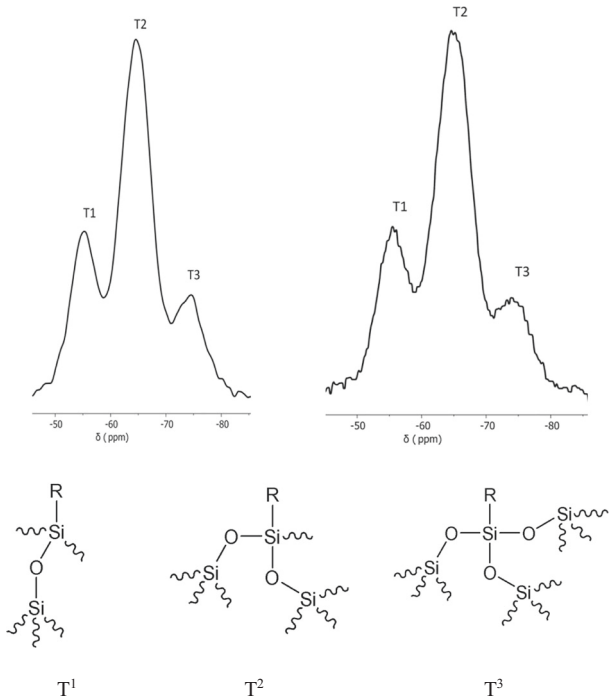

Fig. 4 ^{29}Si CP/MAS ssNMR measurements of BTT and BTP fibres and the structure of the siloxane matrix marked as T^1, T^2 and T^3 units

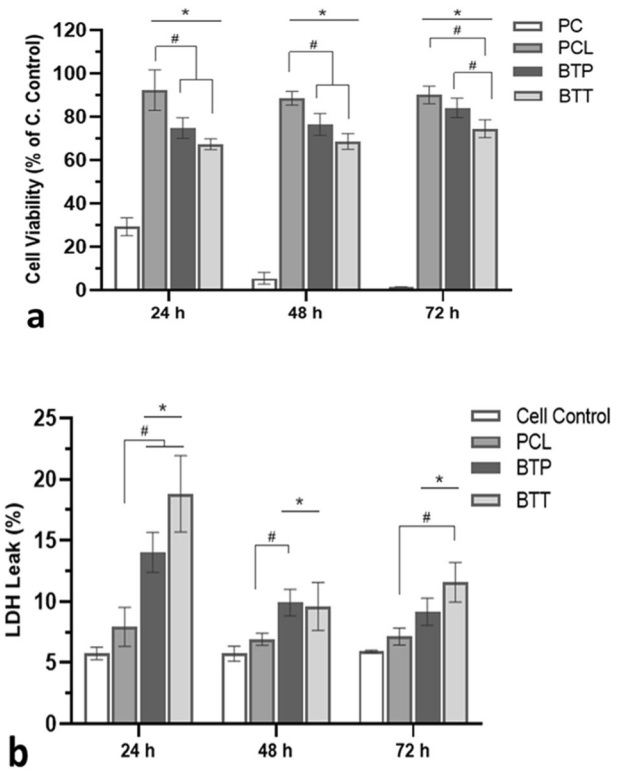

Fig. 5 Impact of nanofibres (PCL, BTP, BTT) on 3T3 fibroblasts (**a**) cell viability and (**b**) membrane disruption (LDH leak). Exposure in direct contact for 24, 48 and 72 hours. Mean ± SD, ANOVA (*) with statistically significant difference to positive control/cell control ($p \leq 0.05$) and (#) between tested nanofibres ($p \leq 0.01$) within the time point

72 hours exposure combined with cell membrane disruption test (LDH leak). As evident from Fig. 5a, the tested samples exhibited significantly higher cell viability in comparison to the positive control (PC) in all time points. Both samples, BTP and BTT showed an increase in cell viability within 72 hours of exposure. The BTP sample can be considered biocompatible for the testing period as it has exceeded 70% viability threshold by exhibiting 74.81 ± 4.79% viability after 24 hours and 84.13 ± 4.50% after 72 hours.

The BTP viability showed no significant difference to PCL control after 72 hours. The BTT sample exhibited 67.32 ± 2.49% viability after 24 hours and 74.52 ± 4.16% after 72 hours. These results can be correlated to the LDH leak results shown in Fig. 5b. Both the tested samples caused significantly increased LDH leak in the first 24 hours (14.02 ± 1.6% BTP, 18.81 ± 3.12% BTT) compared to cell control (CC, 5.75 ± 0.51%) and PCL control (7.92 ± 1.61%).

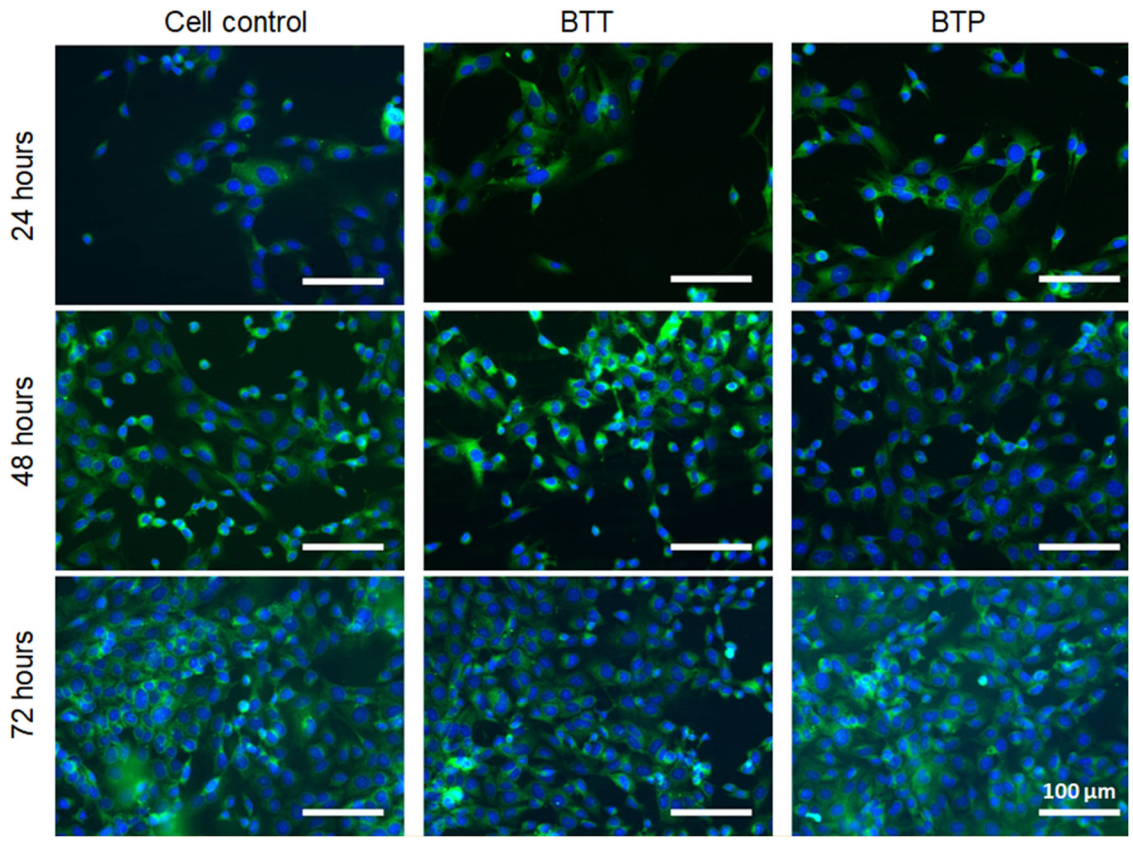

Fig. 6 Fluorescent staining of 3T3 cells morphology development in up to 72 hours exposure. Comparison of untreated cell control BTT and BTP fibres. Visualised by intracellular membrane staining by DiOC6(3) (green) with nuclei counterstained by DAPI (blue). Acquired by Microscope Leica DMi8. Scale bars 100 µm

As evident, the initial cell membrane disruption was stabilised after longer exposure periods and decreased to 9.17 ± 1.12% in the case of BTP after 72 hours, and eventually 11.58 ± 1.63% for BTT. The membrane disruption caused by BTP nanofibres after 72 hours showed no significant difference to PCL nanofibres control at the same time point. None of the values obtained exceeded 20% of LDH leak level. The fluorescent microscopy analysis, see Fig. 6, correlated with the previous quantitative results. Exposure to the BTP nanofibres for 72 hours led to higher cell numbers compared to BTT fibres. The 3T3 cells exhibited a normal spindle-like morphology typical for fibroblastic cells. The appearance was not disrupted after 72 hours of exposure to any tested sample. The obtained results can be related to the surface chemistry and reactivity of the organosilane fibres close to the silica surface chemistry. The LDH release is associated with the membrane integrity of cells, and the membrane lytic potential of certain silane materials was described previously and is often attributed to the surface silanol groups [36, 37]. Although the organosilane materials' surface chemistry is close to the one of silica, the biocompatibility of organosilane materials is improved compared for example to amorphous silica nanoparticles [38]. For example, Shinto et al. documented up to 90% LDH release caused by 2 hours exposure of Jurkat cells to silica nanoparticles. This toxic effect was strongly size and concentration-dependent [39].

3.3.2 In vitro evaluation using ADSC and HUVEC

The cell population density on day 3 after seeding, calculated as the number of cells per cm^2 of the tested materials, showed the possible toxicity of the material and the cell spreading on the material. There was a distinct difference not only within the materials, but within the cell types. The cell population density was nearly two times higher on BTP than on BTT. According to the seeding density (25 000 cell/cm^2), the ADSC on BTP were relatively stabilised on day 3, but on BTT the cell population was significantly decreasing. The images (Figs. 7 and 8) showing cell population density. Each experimental point in graph Fig. 7 was calculated as mean ± SD from 26 to 36 microphotographs. Figure 8 shows the cell nuclei density on the microphotographs, one of each sample group.

To evaluate the cell spreading and basic cell morphology, ADSC were applied on the fibrous samples, cultivated for 3 days, fixed and stained by phalloidin to visualise the F-actin cytoskeleton of the cell. Cell nuclei were counterstained by DAPI.

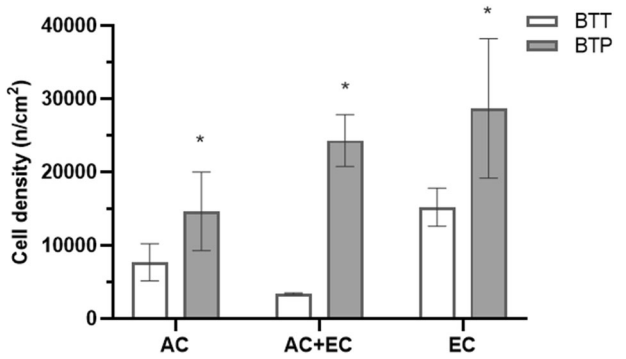

Fig. 7 The cell population density of ADSC (AC), HUVEC (EC) and their cocultivation on materials: BTT and BTP on days 3 after seeding. Each experimental point is calculated as mean ± SD from 4 independent samples (26 to 36 microphotographs). Statistical significance ($p \leq 0.05$) in comparison with other group of samples is marked above the columns (*)

The biocompatibility of BTP treated by ADSC was much higher, then that of BTT. The cell number on the BTP sample reached 14652.8 ± 5321.6 cells/cm^2 compared to 7719.9 ± 2525.1 cells/cm^2 on the BTT after 3 days (see Fig. 7, AC). The ADSC cells colonised the BTP scaffold more densely, their shape was polygonal and elongated (Fig. 9b). The ADSC on BTT were round, badly adhered, and less dense. (Fig. 9a). The HUVEC cells are of smaller size than ADSC, hence by the same degree of construct colonisation, the number of HUVEC is rather higher in comparison with number of ADSCs. After 3 days of cultivation, number of HUVEC cells on BTP material reached 28691 ± 9530.1 cells/cm^2 in contrast to only 15258.7 ± 2598.3 cells/cm^2 on BTT (see Fig. 7, EC).

The metabolic activity of ADSC and endothelial cells on both sample groups was estimated after 24 hours, 48 hours

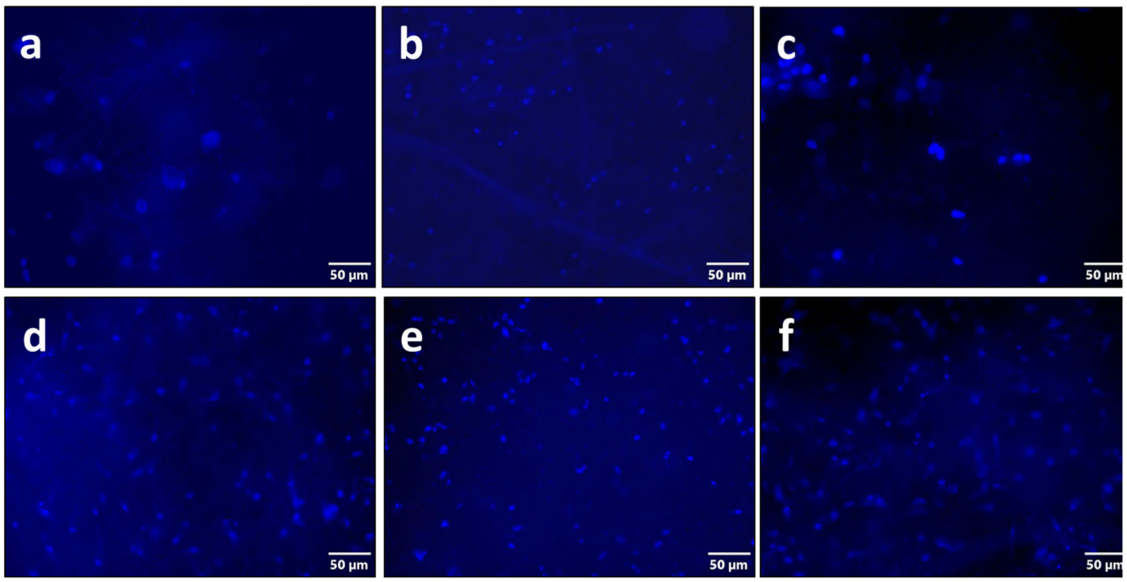

Fig. 8 Visualisation of the cell population density of ADSC (**a**, **d**) and HUVEC (**b**, **e**) and their coculture (**c**, **f**) on materials: BTT (**a**–**c**) and BTP (**d**–**f**) on days 3 after seeding. Cell nuclei stained by DAPI (blue). Fluorescent images were acquired by Microscope Olympus IX71 (digital camera DP71, obj. 20×). Scale bars 50 µm

Fig. 9 Morphology of ADSC seeded on materials: BTT (**a**) and BTP (**b**) visualised by F-actin staining (red). Cell nuclei counterstained by DAPI (blue). Fluorescent images were acquired by Microscope Olympus IX71 (digital camera DP71, obj. 20x)

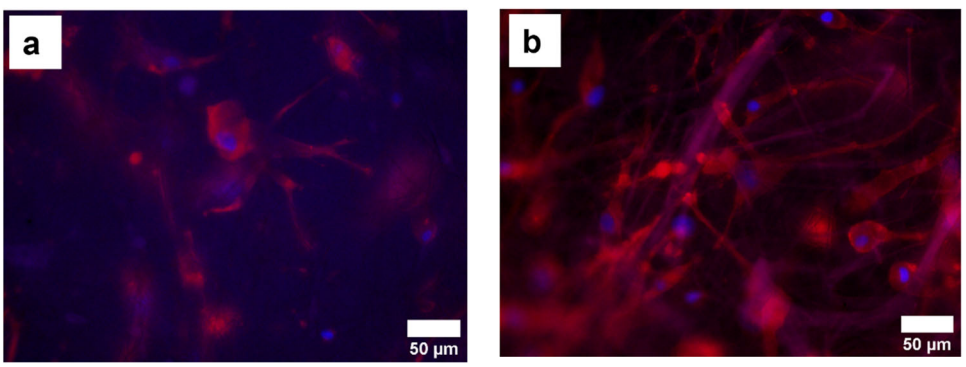

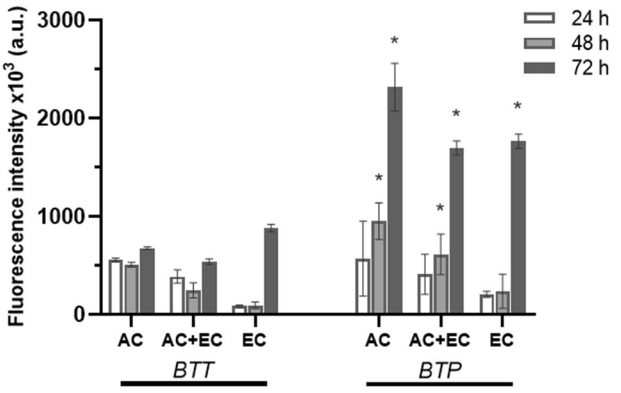

Fig. 10 Metabolic activity of ADSC (AC) and HUVEC endothelial cells (EC), measured by resazurin assay in 72 hours after seeding on materials: BTT, and BTP, Mean ± SD from 4 independent samples. Statistical significance ($p \leq 0.05$) in comparison of both sample groups (*)

and 72 hours to follow the development of the cell growth and survival during this time period. (Fig. 10). The cell metabolic activity of both cell types (ADSC and HUVEC) was rising on BTP, with the highest increment on day 3, after reaching the partial confluence. It shows that supposedly the more specialised endothelial cells adhered and proliferated in the first two days slower, but after this period their metabolic activity was rising faster. The cell metabolic activity on the BTT sample was mostly stabilised in lower values compared to the BTP during this time period. Only the endothelial cells showed significant increase in metabolic activity after 72 hours of cultivation (see Fig. 10, EC (BTT)). Also, the co-cultivation of ADCS with endothelial cells was successful, showing the possible utilisation in soft tissue engineering. In soft tissue prostheses, the smooth muscle cells border with the endothelial cells, moreover, the soft tissues are vascularized by the endothelial cell system, and the scaffold could influence not only the cell growth of individual cell types but their coexistence.

The metabolic test corresponded basically with the cell number obtained on these samples by cell counting and confirmed that the BTP fibres are favoured by both the adipose-derived stem cells (ADSC) cell types.

The interaction of cells with the surface of a biomaterial is one of the key importance for the successful long-term implantation of medical devices [40]. Hence, the hydrophobicity was observed in the case of BTT fibrous material (108° ± 5°). Opposite behaviour was observed within the BTP fibres. The determination of the contact angle proved challenging as the droplet rapidly absorbed into the fibres within a few seconds. This phenomenon suggests a high degree of hydrophilicity, where the fibrous material exhibits a strong affinity and rapid absorption of the liquid, preventing the formation of a distinct droplet shape. The inability to measure a discernible contact angle indicates a significant wettability highlighting the hydrophilic nature of the fibres and their rapid interaction with the liquid phase. Such behaviour is advantageous within regenerative medicine because of the easy adhesion of cells. It is also very beneficial for their survival and further proliferation. In our experiments, the hydrophobicity of the organosilane fibres was partially modified by exposure to ultraviolet light preceding the biological experiment. That could improve the biocompatibility in the case of the more hydrophobic BTT fibrous material. Moreover, the hydrophilic nature of a material can enhances the interaction with a biological system by easier transport of nutrients and interaction with proteins and other biological molecules. Cell adhesion is a fundamental process directly involved in cell growth. Parameters of the tested material such as surface energy, roughness and chemical composition of the surface significantly influence cell's interactions [41].

3.3.3 In vitro evaluation using iPSC derived neural precursors

To evaluate the possible use of developed fibres in the regeneration of the nervous tissue, the neural stem cells were applied to the fibrous samples, cultivated for 3 days and visualised by specific markers nestin (Fig. 11) βIII-tubulin and GFAP (Fig. 12). Cell nuclei were counterstained by DAPI. Cells applied on organosilane fibres make groups and are able to proliferate. Neural precursors colonised BTT only in smaller groups (Fig. 11a), while the BTP fibres were covered more coherently (Fig. 11b).

BTP fibres showed the best results in terms of the ability of neural stem cells to attach to the surface. The cells were evenly distributed on the surface of the sample (Fig. 12a), and they were able to form processes (Fig. 12b). A minority of seeded cells showed a neuron-like morphology and were positive for βIII-tubulin, indicating the beginning of differentiation towards neurons.

4 Discussion

In the construction of biocompatible implants, there are two main strategies, to use and improve the decellularized biological material, as a pure or crosslinked extracellular matrix (ECM), and modulate the cell-material interactions [42], or to develop appropriate artificial materials. In recent years, artificial materials have been of growing importance in medicine and biology. Biomaterials are important for fundamental scientific research as relatively simple and physicochemical well-defined artificial templates of ECM. The possible use of these materials is mostly tested by fibroblasts, and subsequently by stem cells, which are appropriate due to their ability to differentiate into many other cell types. Its non-receptor-mediated cell adhesion on artificial materials means

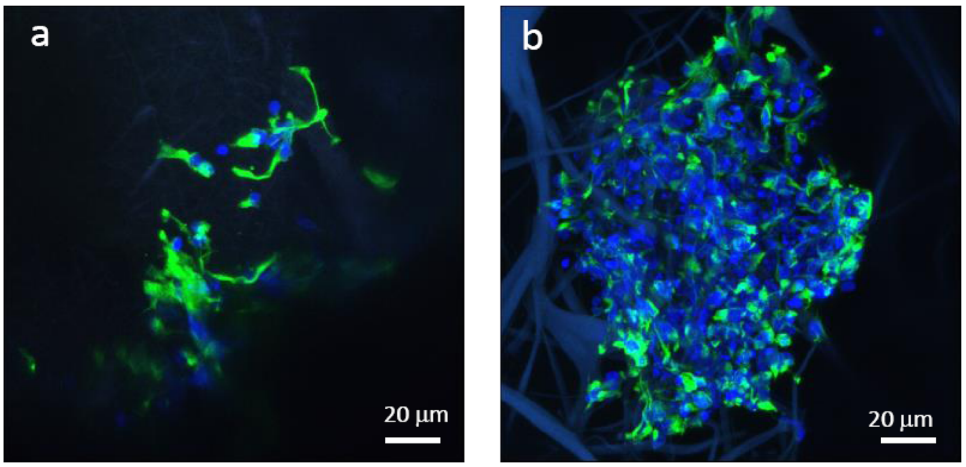

Fig. 11 Morphology of neural stem cells seeded on materials: BTT (**a**) and BTP (**b**) visualised by specific marker nestin (green). Cell nuclei counterstained by DAPI (blue). Fluorescent images were acquired by LSM 810 DUO laser scanning confocal microscope (Zeiss)

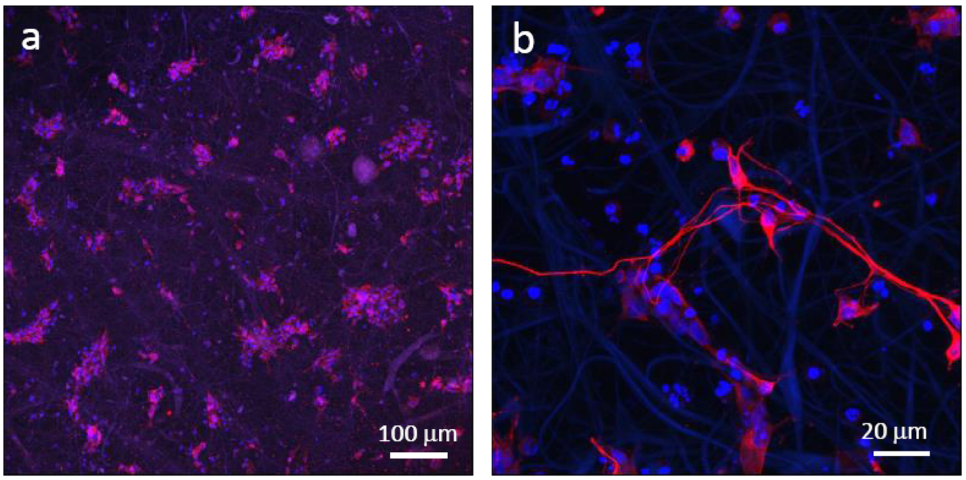

Fig. 12 Morphology of neural stem cells seeded on BTP material visualised by for GFAP (**a**) and βIII-tubulin (**b**), both are red. Cell nuclei counterstained by DAPI (blue). Fluorescent images were acquired by LSM 810 DUO laser scanning confocal microscope (Zeiss)

non-specific cell-material interactions via so-called weak chemical bonding, such as hydrogen bonding, electrostatic, polar or ionic interactions between various molecules on the cell membrane and functional chemical groups the creation of cell-interactive surfaces is markedly influenced by physical and chemical properties of the material surface layer, such as wettability, electrical charge and surface roughness. The optimum protein adsorption and cell adhesion are usually achieved at mild, intermediate values of the surface wettability. Relatively safe, effective and low-cost methods for adjustment of their surface wettability are represented by physical methods, such as ultraviolet light exposure, that we had used for the scaffold sterilisation before the cell seeding.

The development of novel nanofibrous materials for regenerative purposes represents a significant advance in the continually evolving field of regenerative medicine. The crucial factor of our research lies in the use of simple one-pot synthesis together with the electrospinning technique [43]. Thanks to these combinations, the synthesised organosilanes can be effectively transformed into fibrous morphology without the presence of usually toxic solvents or additives such as organic polymers, pore-forming agents or surfactants. The unique combination of inorganic and organic domains connected via strong covalent bonding in the form of nanofibres shows a huge potential in regenerative medicine. Formed BTT and BTP nanofibres state cell viability comparable with already known fibrous biomaterials made from organic or inorganic polymer. Especially the BTP nanofibres showed improved cell adhesion and proliferation compared to pristine silica nanofibres. These are known for their potential applicability as drug delivery systems [44], but require extended surface modification to be able to sustain cell adhesion and proliferation support [45]. Moreover, both developed materials were tested by adipose-derived stem cells and two more specialised cell types. Both tested materials were biocompatible, but supported the cell growth variously. The initial biocompatibility screening on 3T3 murine fibroblasts anticipated better cellular response to the hydrophilic BTP material, encompassing pyridine, which was proven more convenient and more supportive for all tested cell types, revealed the better cell adhesion noticeable from the polygonal cell shape, higher population density, and cell metabolic activity. The ADSCs

and specialised cells as endothelial cells, or neural precursors show a significant preference for the BTP material.

The precise design and engineering of these materials have ushered in a new era of therapeutic possibilities, offering unprecedented precision and effectiveness in tissue repair and regeneration. The unique properties of nanofibrous materials, including their high surface area, porosity and biomimetic characteristics, have positioned them as indispensable tools in fostering cellular responses crucial for successful regenerative outcomes. The possible ability of these materials to mimic the extracellular matrix on a nanoscale range and provide a supportive framework for cellular growth underscores their potential across neuroregenerative medicine.

5 Conclusion

The combination of one-pot synthesis and electrospinning techniques has facilitated the production of innovative pure hybrid organosilane nanofibres with unique properties, eliminating the need for potentially harmful additives through the process. Among these, BTP nanofibres demonstrate superior biocompatibility and enhanced support for cell adhesion, proliferation, and metabolic activity, making them promising for applications in tissue repair and regeneration. Their ability to mimic the extracellular matrix and foster cellular responses highlights their potential in diverse fields, including neuroregenerative medicine and drug delivery systems. This research underscores the transformative potential of precisely engineered biomaterials in advancing therapeutic possibilities.

Acknowledgements This research was supported by the European Union—European Structural and Investment Funds in the framework of the Operational Programme Research, Development, and Education project "Hybrid Materials for Hierarchical Structures (HyHi)", Reg. No. CZ.02.1.01/0.0/0.0/16_019/0000843. The authors acknowledge the assistance provided by the Research Infrastructure NanoEnviCz, supported by the Ministry of Education, Youth and Sports of the Czech Republic under Project No. LM2018124. This work was also supported by the Student Grant Competition of the Technical University of Liberec under project No. SGS-2022-4059, and by the project No. CZ.02.01.01/00/22_008/0004562 of the Ministry of Education, Youth and Sports, co-funded by the European Union.

Compliance with ethical standards

Conflict of interest The authors declare no competing interests.

Publisher's note Springer Nature remains neutral with regard to jurisdictional claims in published maps and institutional affiliations.

References

1. Roth JG, Huang MS, Li TL, Feig VR, Jiang Y, Cui B, et al. Advancing models of neural development with biomaterials. Nat Rev Neurosci. 2021;22:593–615. https://doi.org/10.1038/s41583-021-00496-y
2. George PM, Bliss TM, Hua T, Lee A, Oh B, Levinson A, et al. Electrical preconditioning of stem cells with a conductive polymer scaffold enhances stroke recovery. Biomaterials. 2017;142:31–40. https://doi.org/10.1016/j.biomaterials.2017.07.020
3. Gould E, Reeves AJ, Fallah M, Tanapat P, Gross CG, Fuchs E. Hippocampal neurogenesis in adult Old World primates. Proc Natl Acad Sci USA. 1999;96:5263–7. https://doi.org/10.1073/pnas.96.9.5263
4. Alvarez-Buylla A, Kirn JR. Birth, migration, incorporation, and death of vocal control neurons in adult songbirds. J Neurobiol. 1997;33:585–601.
5. Sugaya K. Neuroreplacement therapy and stem cell biology under disease conditions. CMLS, Cell Mol Life Sci. 2003;60:1891–902. https://doi.org/10.1007/s00018-002-3014-y
6. Teixeira FG, Carvalho MM, Sousa N, Salgado AJ. Mesenchymal stem cells secretome: a new paradigm for central nervous system regeneration? Cell Mol Life Sci. 2013;70:3871–82. https://doi.org/10.1007/s00018-013-1290-8
7. Basak S. Redesigning the modern applied medical sciences and engineering with shape memory polymers. Adv Compos Hybrid Mater. 2021;4:223–34. https://doi.org/10.1007/s42114-021-00216-1
8. Nagappan PG, Chen H, Wang D-Y. Neuroregeneration and plasticity: a review of the physiological mechanisms for achieving functional recovery postinjury. Military Med Res. 2020;7:30. https://doi.org/10.1186/s40779-020-00259-3
9. Abbas WA, Ibrahim ME, El-Naggar M, Abass WA, Abdullah IH, Awad BI, et al. Recent advances in the regenerative approaches for traumatic spinal cord injury: materials perspective. ACS Biomater Sci Eng. 2020;6:6490–509. https://doi.org/10.1021/acsbiomaterials.0c01074
10. Balint R, Cassidy NJ, Cartmell SH. Conductive polymers: Towards a smart biomaterial for tissue engineering. Acta Biomaterialia. 2014;10:2341–53. https://doi.org/10.1016/j.actbio.2014.02.015
11. Song S. Controlling properties of human neural progenitor cells using 2D and 3D conductive polymer scaffolds. Sci Rep. 2019;9:19565. https://doi.org/10.1038/s41598-019-56021-w
12. Kaur G, Adhikari R, Cass P, Bown M, Gunatillake P. Electrically conductive polymers and composites for biomedical applications. RSC Adv. 2015;5:37553–67. https://doi.org/10.1039/C5RA01851J
13. Escobar A, Serafin A, Carvalho MR, Culebras M, Cantarero A, Beaucamp A, et al. Electroconductive poly(3,4-ethylenedioxythiophene) (PEDOT) nanoparticle-loaded silk fibroin biocomposite conduits for peripheral nerve regeneration. Adv Compos Hybrid Mater. 2023;6:118. https://doi.org/10.1007/s42114-023-00689-2
14. Mao J, Zhang Z. Polypyrrole as electrically conductive biomaterials: synthesis, biofunctionalization, potential applications and

challenges. Adv Exp Med Biol. 2018;1078:347–70. https://doi.org/10.1007/978-981-13-0950-2_18
15. Shin SR, Li Y-C, Jang HL, Khoshakhlagh P, Akbari M, Nasajpour A, et al. Graphene-based materials for tissue engineering. Adv Drug Del Rev. 2016;105:255–74. https://doi.org/10.1016/j.addr.2016.03.007
16. Kim C-H, Lee S-Y, Rhee KY, Park S-J. Carbon-based composites in biomedical applications: a comprehensive review of properties, applications, and future directions. Adv Compos Hybrid Mater. 2024;7:55. https://doi.org/10.1007/s42114-024-00846-1
17. Fadeel B, Kostarelos K. Grouping all carbon nanotubes into a single substance category is scientifically unjustified. Nat Nanotechnol. 2020;15:164–164. https://doi.org/10.1038/s41565-020-0654-0
18. Lalwani G, D'Agati M, Khan AM, Sitharaman B. Toxicology of graphene-based nanomaterials. Adv Drug Del Rev. 2016;105:109–44. https://doi.org/10.1016/j.addr.2016.04.028
19. Voge CM, Stegemann JP. Carbon nanotubes in neural interfacing applications. J Neural Eng. 2011;8:011001. https://doi.org/10.1088/1741-2560/8/1/011001
20. Vashist A, Kaushik A, Vashist A, Sagar V, Ghosal A, Gupta YK, et al. Advances in carbon nanotubes-hydrogel hybrids in nanomedicine for therapeutics. Adv Healthc Mater. 2018;7:e1701213. https://doi.org/10.1002/adhm.201701213
21. Liang Y, Qiao L, Qiao B, Guo B. Conductive hydrogels for tissue repair. Chem Sci. 2023;14:3091–116. https://doi.org/10.1039/D3SC00145H
22. Choi S, Raja IS, Selvaraj AR, Kang MS, Park T-E, Kim KS, et al. Activated carbon nanofiber nanoparticles incorporated electrospun polycaprolactone scaffolds to promote fibroblast behaviors for application to skin tissue engineering. Adv Compos Hybrid Mater. 2023;6:24. https://doi.org/10.1007/s42114-022-00608-x
23. Mendes P M. Cellular nanotechnology: making biological interfaces smarter. Chem Soc Rev. 2013;42:9207–18. https://doi.org/10.1039/C3CS60198F
24. Chen J, Zhang G, Zhao Y, Zhou M, Zhong A, Sun J. Promotion of skin regeneration through co-axial electrospun fibers loaded with basic fibroblast growth factor. Adv Compos Hybrid Mater. 2022;5:1111–25. https://doi.org/10.1007/s42114-022-00439-w
25. Verma S, Domb AJ, Kumar N. Nanomaterials for regenerative medicine. Nanomedicine. 2011;6:157–81. https://doi.org/10.2217/nnm.10.146
26. Biazar E, Khorasani M, Montazeri N, Pourshamsian K, Daliri M, MR T, et al. Types of neural guides and using nanotechnology for peripheral nerve reconstruction. Int J Nanomed. 2010;5:839–52. https://doi.org/10.2147/IJN.S11883
27. Basu B (2020) Crossing the Boundaries. In: Biomaterials Science and Implants: Status, Challenges and Recommendations. Springer, Singapore, pp 1–27
28. Holubová B, Máková V, Müllerová J, Brus J, Havlíčková K, Jenčová V, et al. Novel chapter in hybrid materials: One-pot synthesis of purely organosilane fibers. Polymer. 2020;190:122234. https://doi.org/10.1016/j.polymer.2020.122234
29. Travnickova M, Pajorova J, Zarubova J, Krocilova N, Molitor M, Bacakova L. The influence of negative pressure and of the harvesting site on the characteristics of human adipose tissue-derived stromal cells from lipoaspirates. Stem Cells Int. 2020;2020:e1016231. https://doi.org/10.1155/2020/1016231
30. Yu J, Vodyanik MA, Smuga-Otto K, Antosiewicz-Bourget J, Frane JL, Tian S, et al. Induced pluripotent stem cell lines derived from human somatic cells. Science. 2007;318:1917–20. https://doi.org/10.1126/science.1151526
31. Polentes J, Jendelova P, Cailleret M, Braun H, Romanyuk N, Tropel P, et al. Human induced pluripotent stem cells improve stroke outcome and reduce secondary degeneration in the recipient brain. Cell Transplant. 2012;21:2587–602. https://doi.org/10.3727/096368912X653228
32. Máková V, Holubová B, Krabicová I, Kulhánková J, Řezanka M. Hybrid organosilane fibrous materials and their contribution to modern science. Polymer. 2021;228. https://doi.org/10.1016/j.polymer.2021.123862
33. Brinker CJ. Hydrolysis and condensation of silicates: Effects on structure. J Non-Crystalline Solids. 1988;100:31–50. https://doi.org/10.1016/0022-3093(88)90005-1
34. Jiang H, Zheng Z, Wang X. Kinetic study of methyltriethoxysilane (MTES) hydrolysis by FTIR spectroscopy under different temperatures and solvents. Vibrational Spectroscopy. 2008;1:1–7. https://doi.org/10.1016/j.vibspec.2007.07.002
35. Tejedor-Tejedor MI, Paredes L, Anderson MA. Evaluation of ATR−FTIR Spectroscopy as an "in Situ" tool for following the hydrolysis and condensation of alkoxysilanes under rich H2O Conditions. Chem Mater. 1998;10:3410–21. https://doi.org/10.1021/cm980146l
36. Pavan C, Delle Piane M, Gullo M, Filippi F, Fubini B, Hoet P, et al. The puzzling issue of silica toxicity: are silanols bridging the gaps between surface states and pathogenicity?. Particle Fibre Toxicol. 2019;16:32–41. https://doi.org/10.1186/s12989-019-0315-3
37. Morais R, Hochheim S, Camargo de Oliveira C, Riegel-Vidotti I, Marino C. Skin interaction, permeation, and toxicity of silica nanoparticles: Challenges and recent therapeutic and cosmetic advances. International Journal Pharmaceutics. 2022;614:121439. https://doi.org/10.1016/j.ijpharm.2021.121439
38. Máková V, Holubová B, Tetour D, Brus J, Řezanka M, Rysová M, et al. (1S,2S)-Cyclohexane-1,2-diamine-based Organosilane Fibres as a Powerful Tool Against Pathogenic Bacteria. Polymers. 2020;12:206. https://doi.org/10.3390/polym12010206
39. Shinto H, Fukasawa T, Yoshisue K, Tezuka M, Orita M. Cell membrane disruption induced by amorphous silica nanoparticles in erythrocytes, lymphocytes, malignant melanocytes, and macrophages. Adv Powder Technol. 2014;25:1872–81. https://doi.org/10.1016/j.apt.2014.09.002
40. Dowling DP, Miller IS, Ardhaoui M, Gallagher WM. Effect of surface wettability and topography on the adhesion of osteosarcoma cells on plasma-modified polystyrene. J Biomater Appl. 2011;26:327–47. https://doi.org/10.1177/0885328210372148
41. Meyer U, Szulczewski D, Moeller K, Heide H, Jones D. Attachment kinetics and differentiations of osteoblasts on different biomaterials. Cells Mater. 1993;3:129–40.
42. Musilkova J, Filova E, Pala J, Matejka R, Hadraba D, Vondrasek D, et al. Human decellularized and crosslinked pericardium coated with bioactive molecular assemblies. Biomed Mater. 2019;15:015008. https://doi.org/10.1088/1748-605X/ab52db
43. Hobbs C, Kulhánková J, Nikendey Holubová B, Mahun A, Kobera L, Erben J, et al. Hybrid organosilane nanofibre scaffold formation supporting cell adhesion and growth. J Mater Sci. 2024;59:19612–27. https://doi.org/10.1007/s10853-024-10324-0
44. Danilová I, Lovětinská-Šlamborová I, Máková V, Voleský L, Rysová M. Immobilization of esterase enzyme onto silica nanofibers for biomedical applications. Vlakna a Textil. 2014;21:3–11.
45. Steinerova M, Matejka R, Stepanovska J, Filova E, Stankova L, Rysova M, et al. Human osteoblast-like SAOS-2 cells on submicron-scale fibers coated with nanocrystalline diamond films. Mater Sci Eng: C. 2021;121:111792. https://doi.org/10.1016/j.msec.2020.111792